Electronic Supplementary Information (ESI)

Trace Ethylene Carbonate Mediated Low-Concentration Ether-based Electrolytes for High-Voltage Lithium Metal Batteries

Yinghua Chen,[ab] Zheng Ma,[a] Yuqi Wang,[a] Pushpendra Kumar,[c] Fei Zhao,[a] Tao Cai,[a] Zhen Cao,[d] Luigi Cavallo,[d] Haoran Cheng,[a] Qian Li[a] and Jun Ming*[ab]

[a]State Key Laboratory of Rare Earth Resource Utilization, Changchun Institute of Applied Chemistry, Chinese Academy of Sciences, Changchun, 130022, China

[b]School of Applied Chemistry and Engineering, University of Science and Technology of China, Hefei, 230026, China

[c]School of Physical Sciences, Jawaharlal Nehru University, New Delhi 110067, India

[d]KAUST Catalysis Center, King Abdullah University of Science and Technology (KAUST), Thuwal 23955-6900, Saudi Arabia

* To whom correspondence should be addressed: jun.ming@ciac.ac.cn.

Experimental Section

Materials. 1,2-Dimethoxyethane (DME, battery-grade), ethylene carbonate (EC, battery-grade), propylene carbonate (PC), fluoroethylene carbonate (FEC), lithium hexafluorophosphate ($LiPF_6$, battery-grade) and lithium perchlorate ($LiClO_4$, battery-grade) were provided from *DodoChem Co., Ltd.* Lithium nitrate ($LiNO_3$, battery-grade) and KS-6 were purchased from *Guangdong Canrd New Energy Technology Co., Ltd.* Nmethyl-2pyrrolidone (NMP, >99.0%) was purchased from *Aladdin*. The polyvinylidene fluoride (PVDF) and Super C45 were purchased from *HF-Kejing*. All reagents were used directly without further purification.

Electrolyte and electrode preparation. Electrolyte solutions were prepared by mixing a given amount of $LiPF_6$ with solvents in an Ar-filled glove box, in which the content of O_2 and H_2O was maintained below 3.0 ppm. Different electrolytes were formulated in molar ratio as $LiPF_6$: DME (1: 21) and $LiPF_6$: EC: DME (1: 0.3: 15), respectively, which are abbreviated as the LD and LED electrolytes accordingly. The LP57 electrolyte was composed of 1.0 M $LiPF_6$ in a mixture of ethylene carbonate (EC) and ethyl methyl carbonate (EMC) in a weight ratio of 3:7. The $LiNi_{0.8}Co_{0.1}Mn_{0.1}O_2$ (NCM811) was purchased from *Rongbai Technology*. Lithium foils (500 μm in thickness) and Lithium foils (100 μm in thickness) were purchased from *China Energy Lithium Co., Ltd.* The average thickness of 100 μm lithium foil after rolling is 80 μm. The cathode was prepared by mixing NCM811, Super C45, KS-6, and polyvinylidene fluoride binder with a mass ratio of 90: 2.5: 2.5: 5 in N-methyl-2-pyrrolidone. The mixtures were milled with a Hasai planetary mixer for 5 min. Then, the uniform cathode slurry was coated on the Al current collector. Finally, the NCM811 electrodes were dried at 80 °C in a vacuum for 12 h before assembling the cell. The loading of the cathode was controlled at about ~7.0 mg cm^{-2}.

Electrochemical Measurements. All the batteries were assembled using the 2025-type coin cell with a polypropylene (PP) separator (*Celgard 2400*) and disassembled in an argon-filled glove box. The Li || NCM811 cell was assembled by using the cathode and Li metal anode with a thickness of 500 μm or 80 μm and 50 μl electrolyte was used. All the cells were charged to 4.5 V vs. Li/Li^+ and then discharged to 2.8 V at 0.1 C in the initial two cycles. Then, the constant current (CC) protocol was applied in the normal cycling and rate test. After the above activation process (i.e., two cycles at 0.1 C and two cycles at 0.2 C), the cells were cycled at 0.5 C for long cycling or performed power capacity at different rates (i.e., 0.5 C, 1.0 C, 1.5 C, and 2.0 C). The Li || Li symmetrical cells were comprised of two Li metal pieces (13.6 mm in diameter) in the 2032-type coin cell. Long-term galvanostatic cycling was performed at 0.5 mA cm^{-2} with a

certain cut-off capacity of 1 mAh cm^{-2}. All (dis-)charge curves were recorded by the Neware instrument.

In the linear sweep voltammetry (LSV) test, cells are assembled using aluminum foil with a diameter of 12 μm. The voltage window was set from 3.0 to 6.0 V using a scan rate of 1 mV s^{-1}. In addition, the leakage currents of NCM811 cathodes were performed under a constant voltage of 4.5 V (vs. Li/Li^+) after cycling in different electrolytes for three cycles under 0.2 C. Besides, the electrochemical impedance spectroscopy (EIS) measurements were conducted between a frequency range of 300 kHz and 10 mHz and a sinusoidal amplitude of 10 mV. The electrodes of the symmetrical cell, such as the NCM811 || NCM811 and Li || Li cell, were obtained from the Li || NCM811 cells that were discharged at the stage of 50% of the depth of discharge (DOD) in a cell after the 20 cycling. All curves were acquired by the electrochemical station *Bio-Logic VMP3*.

The de-solvation energy barrier can be calculated through the Arrhenius equation (equation (1), (2)), and relevant information needs to be obtained by measuring the electrochemical impedance spectra (EIS) of Li || NCM811 cells at different temperatures (from 253 to 293 K),

$$k = \frac{T}{R_{EIS}} = Ae^{-E_a/RT} \tag{1}$$

$$\ln\left(\frac{T}{R_{EIS}}\right) = lnA - \frac{E_a}{R} \cdot \frac{1}{T} \tag{2}$$

where k is the rate constant, T is the absolute temperature, R_{EIS} is the measured electrochemical impedance, A is the pre-exponential factor, E_a is the activation energy, and R is the standard gas constant.[1] The charge transfer impedance obtained by fitting from the impedance spectrum is substituted into Equation 2. R_{ct} represents the Li^+ desolvation resistance at the electrode/electrolyte interface at low frequency (also represents the charge transfer impedance).

Electrolyte characterizations. The Fourier transform infrared (FTIR) spectrum was acquired by the Nicolet 6700 FT-IR spectrometer with 2 cm^{-1} resolution and a total of 32 times scans. All FTIR spectra were analyzed by OMNIC and Originlab software. In the nuclear magnetic resonance (NMR) tests, a coaxial internal insert that contained a standard NMR solution (i.e., 0.1 mol kg^{-1} $LiPF_6$ in 1 wt% H_2O + 1 wt% C_2H_5OH + 98 wt% D_2O as the reference) was inserted into the NMR tube to analyze the pristine microstructure of electrolyte by a Bruker AVIII 400 MHz Liquid NMR spectrometer. In Heteronuclear Overhauser Effect Spectroscopy (HOESY) tests, the standard solution in the coaxial internal insert is $LiPF_6$: FEC: PC (1 : 5 : 7,

mol ratio) and 1.5 times the volume of deuterated benzene (C_6D_6). Note that all HOESY tests use the same coaxial tube and sample tube, with only the electrolyte being changed. The solvent-solvent interaction (i.e., PC-H and FEC-F) between polar molecules in the external calibration solution was selected as a reference. The strength of the solvent-solvent interactions within the external calibration solutions sealed in the coaxial tube remains constant, making it suitable as a Reference for quantitative analysis. This approach aims to ensure that the Reference remains a constant quantity during 2D HOESY quantitative analysis of changes in anion-solvent interaction.

The conductivity of electrolytes was measured on a conductivity meter (Five Easy PlusTM-FE38, Mettler Toledo Co., Ltd) at 25°C. To measure the lithium-ion (Li^+) transference number, the Li||Li symmetrical cells were assembled and pre-cycled at a small current of 0.03 mA. Then, a 10 mV (ΔV) direct current (DC) pulse was applied to the Li||Li symmetrical cells for 10 min to obtain the initial currents of I_0 and I_{ss} when the current reached a steady state. The EIS test was acquired before (R_0) and after (R_{ss}) the polarization between a frequency range from 300 kHz to 100 mHz by a sinusoidal amplitude of 10 mV. Then, the transference number was calculated using the equation

$$t^+ = \frac{I_{ss}(\Delta V - I_0 R_0)}{I_0(\Delta V - I_{ss} R_{ss})} \quad (3)$$

where ΔV is the applied polarization voltage and I_0 and I_{ss} are the initial current and steady-state current before and after polarization, respectively. Correspondingly, R_0 and R_{ss} are the initial interfacial resistance and interfacial resistance after 600 s of polarization, respectively. The conductivity of electrolytes was measured on a conductivity meter (Five Easy PlusTM-FE38, Mettler Toledo Co., Ltd.) at 25 °C.

Electrode characterizations. The morphology of the cycled electrodes was characterized by scanning electron microscopy (SEM, Hitachi S-4800). The XPS spectra of the electrodes were performed by X-ray photoelectron spectroscopy (XPS, ESCALABMKLL). All the cycled electrodes were rinsed with pure anhydrous DME solvent to remove residual $LiPF_6$, dried, and then sealed in the glovebox before being transferred for characterizations. Time-of-flight secondary ion mass spectrometry (TOF-SIMS) analysis was performed by a TOF-SIMS. 5 Spectrometer (ION-TOF GmbH). All detected secondary ions of interest had a mass resolution of > 5000 and a pulsed 30 keV Bi^+ ion beam was employed for depth profiling and a 1 keV Cs^+ ion beam was utilized for the sputtering of the cycled electrodes with a typical sputtered area (200 μm × 200 μm). The total sputter time was 1000 s.

Theoretical simulation. Quantum chemistry calculations were first performed to optimize molecular geometries of DME and EC solvent molecules using the Gaussian 16 package[1] at B3LYP/6-311+G(d,p) level of theory. The atomic partial charges on these solvent molecules were calculated using the ChelpG method at the same level of theory (the B3LYP hybrid functional and the 6-311+G(d,p) basis set). The atomistic force field parameters for all ions and molecules are described in the AMBER format and are taken from a previous work.[3] The cross-interaction parameters between different atom types are obtained from the Lorentz-Berthelot combination rule.

Two modelling systems were constructed, and the detailed system compositions are listed in **Table S1**. All atomistic simulations were performed using the GROMACS package with cubic periodic boundary conditions.[4] The equations for the motion of all atoms were integrated using a classic Verlet leapfrog integration algorithm with a time step of 1.0 fs. A cutoff radius of 1.6 nm was set for short-range van der Waals interactions and real-space electrostatic interactions. The particle-mesh Ewald (PME) summation method with an interpolation order of 5 and a Fourier grid spacing of 0.20 nm was employed to handle long-range electrostatic interactions in reciprocal space. All simulation systems were first energetically minimized using a steepest descent algorithm, and thereafter annealed gradually from 600 K to room temperature (300 K) within 10 ns. All annealed simulation systems were equilibrated in an isothermal-isobaric (NPT) ensemble for 20 ns of physical time maintained using a Nosé-Hoover thermostat and a Parrinello-Rahman barostat with time coupling constants of 0.4 and 0.2 ps, respectively, to control the temperature at 300 K and the pressure at 1 atm. Atomistic simulations were further performed in a canonical ensemble (NVT) for 50 ns, and simulation trajectories were recorded at an interval of 100 fs for further structural and dynamical analysis.

Representative solvation structures were extracted from extensive atomistic simulations, and these solvation structures were adopted as starting configurations for additional DFT calculations. DFT calculations were performed using the Gaussian 16 software[2] at the same level of theory (B3LYP/6-311+G(d)) and with Grimme's-D3 (gd3bj) dispersion correction to obtain the optimized coordination structures, and thereafter to calculate the binding energies and LUMO-HOMO energies for representative solvation structures.

Calculation method of reaction free energy of dissolution process.[5] In this system, the x, y and Z dimensions were periodic boundary conditions. The OPLS force field, which is suitable for the electrolyte solution, was used to optimize sample structures for preliminary structural optimization. Atomic charges of ions were multiplied by a scale factor of 0.73 to correct the

polarization effect of anion and cation. First, the conjugate gradient algorithm and energy minimization were performed to obtain a stable structure before using dynamic simulations. Each sample was then equilibrated under the NPT ensemble at a constant temperature of 400 K to achieve an equilibrium state with zero pressure for 5 ns. Subsequently, the system temperature was reduced from 400 K to 298 K for annealing 5 ns under the NPT ensemble (under 1 atmosphere). The Andersen feedback thermostat and Berendsen barostat algorithm were applied in the system with temperature and pressure conversion. Next, MD simulations were further carried out for 10 ns with a time step of 1 fs per integration step under the ensemble conditions of NVT (298 K). System energy can be obtained through structural optimization using energy minimization. The energy barriers were examined by linear and quadratic synchronous transit methods in combination with the conjugated gradient (CG) refinement. The free energies were obtained by $G = E_{total} + E_{ZPE} - TS$, where E_{total}, $E_{ZPE,}$ and TS are the ground-state energy, zero-point energies, and entropy terms, respectively, with the latter two taking vibration frequencies from DFT. Finally, the reaction energies (G) of different intermediates are defined as $\Delta G = G_i - G_{reactant}$ (G_i is the energy of intermediates and $G_{reactant}$ is the total energy of the reactants). Note that the dissociation energy ($\Delta G_{dissociation}$) refers to the energy required to break down 1 mol of salt into completely separated free ions and bring them into perfect contact with 1 mol of solvent molecules. The solvation energy ($\Delta G_{solvation}$) denotes the energy released when 1 mol of these completely separated free ions interacts with solvent molecules and forms a complex until they are fully solvated.

Table S1 Constructed modelling systems and the detailed system compositions.

Kinds of species	LD	LED
Li^+-PF_6^-	45	65
DME	990	975
EC		20
Total No. of atoms	16200	16320
Simulation system size	$(5.5476\ nm)^3$	$(5.5711\ nm)^3$

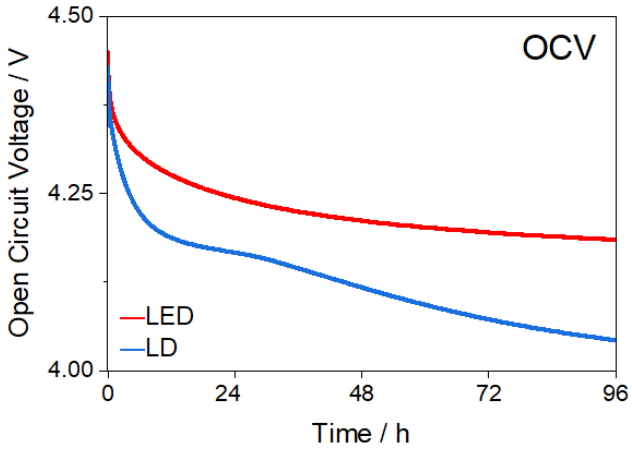

Fig. S1 Evolution of OCV for Li || NCM811 cell when charged to 4.5 V.

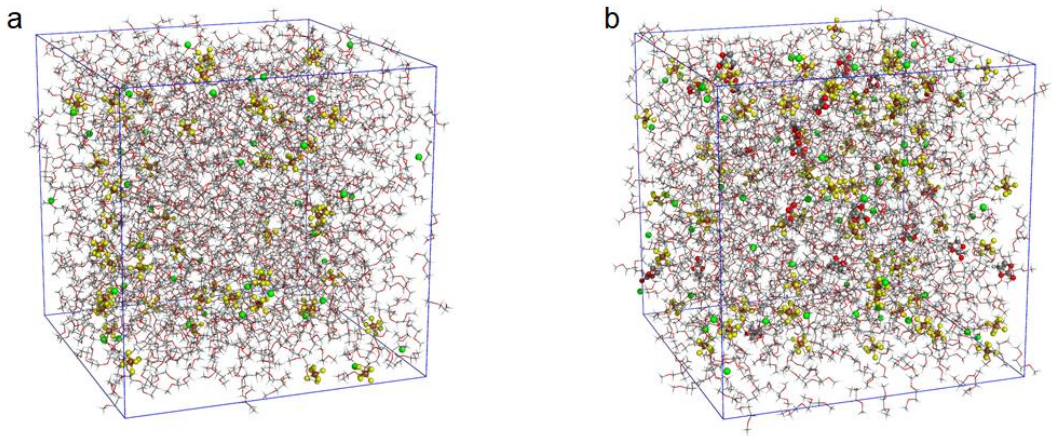

Fig. S2 Snapshots of (a) LD and (b) LED electrolytes given by MD simulation boxes.

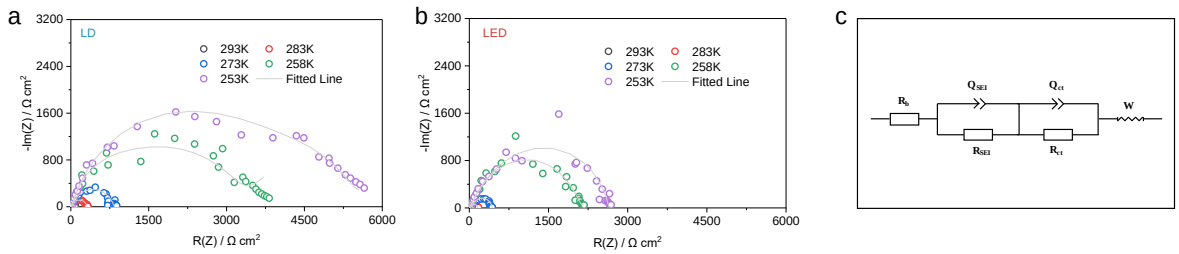

Fig. S3 Nyquist plots and EIS fitting process of Li || NCM811 cells when plating and stripping from 253 K to 293 K in (a) LD, and (b) LED electrolytes. (c) Equivalent circuit of above EIS fitting.

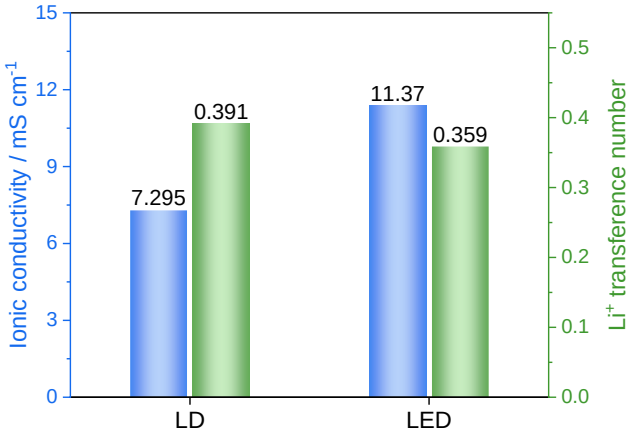

Fig. S4 Ionic conductivity (blue) and Li^+ transference number (green) of different electrolytes. The ionic conductivity of the LED electrolyte is higher than that of the LD electrolyte, which further demonstrates that the presence of EC can facilitate the dissociation of the Li^+/PF_6^- effectively. Moreover, the Li^+ transference number of the LED electrolyte is slightly lower than that in the LD electrolyte, which further verifies that the presence of EC can strengthen the interaction between Li^+ and PF_6^- ions within the electrolyte, resulting in the increased amount of the CIPs. The higher ionic conductivity in the LED electrolyte can reduce the concentration polarization significantly, even though the Li^+ transference number is slightly lower. Thus, it does not conflict with its excellent electrochemical performance. In contrast, although the LD electrolyte displays a slightly higher Li^+ transference number, its lower ionic conductivity can lead to pronounced concentration polarization. This, in turn, could result in the irreversible deposition of Li^+ on the anode and an accumulation of anions on the cathode surface, thereby increasing the probability of decomposition and expiry of the battery.

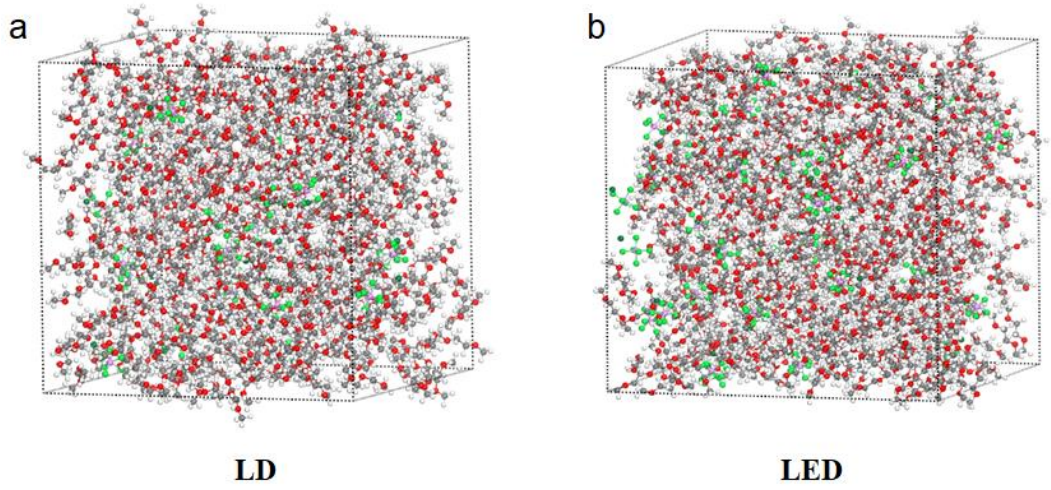

Fig. S5 Snapshots of (a) LD and (b) LED electrolytes given by MD simulation boxes for reaction-free energy.

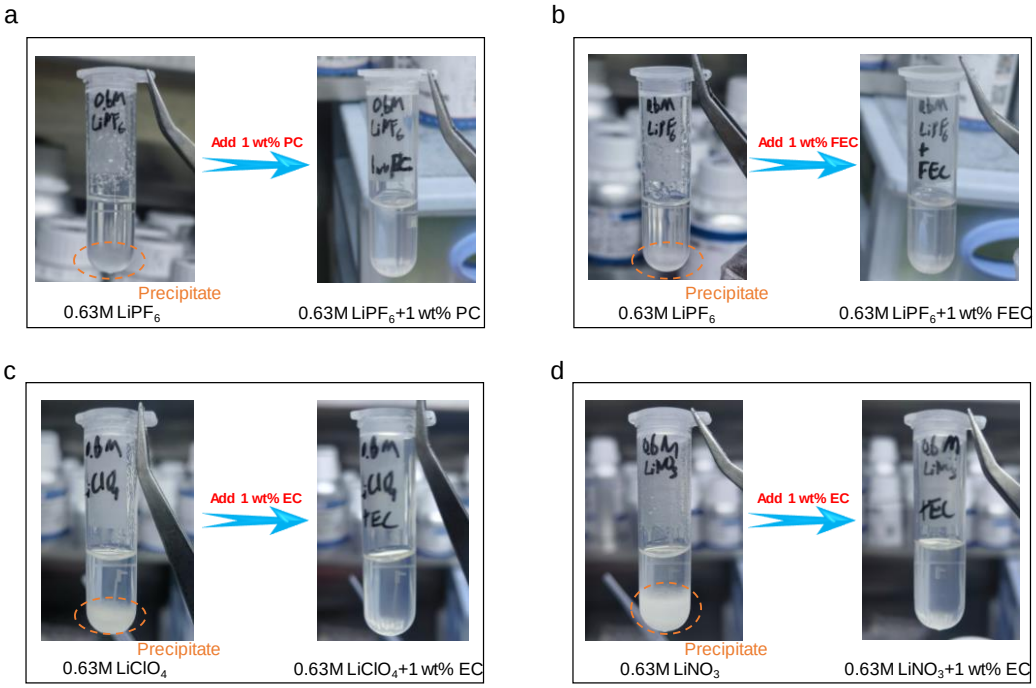

Fig. S6 Digital images of the (a) PC and (b) FEC solubilization effect of $LiPF_6$ in DME. Digital images of the EC solubilization effect of (c) $LiClO_4$ and (d) $LiNO_3$ in DME.

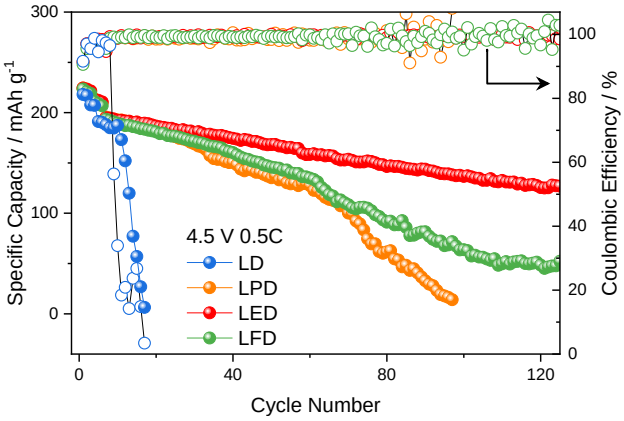

Fig. S7 Comparative cycle performance of 0.63 M $LiPF_6$ dissolved in DME with 1 wt% of each cyclic carbonate solvent for the Li|NCM811 half-cell operated at the conditions of 4.5 V at 0.5C. The abbreviation of LPD, LED, and LFD electrolyte correspond to the DME-based electrolyte containing 0.63 M LiPF6 with 1 wt% of PC, EC, and FEC, respectively. The addition of trace amounts of cyclic carbonate solvent can not only significantly improve the solubility of $LiPF_6$, but also improve the cycle performance of the electrolyte in the Li|NCM811 half-cell.

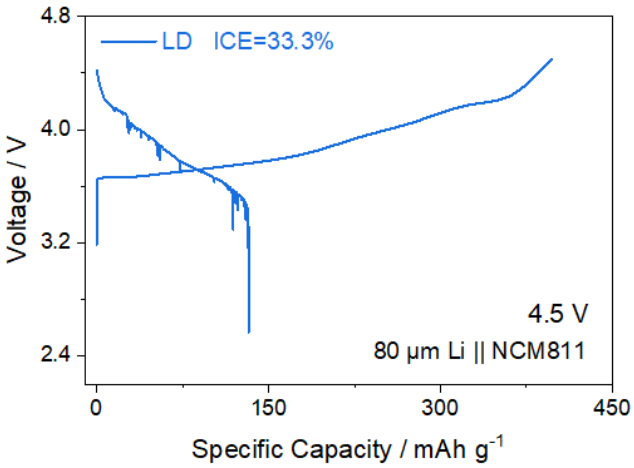

Fig. S8 The initial charge and discharge curves under 4.5 V of 80 μm Li || NCM811 full-cell in LD electrolyte.

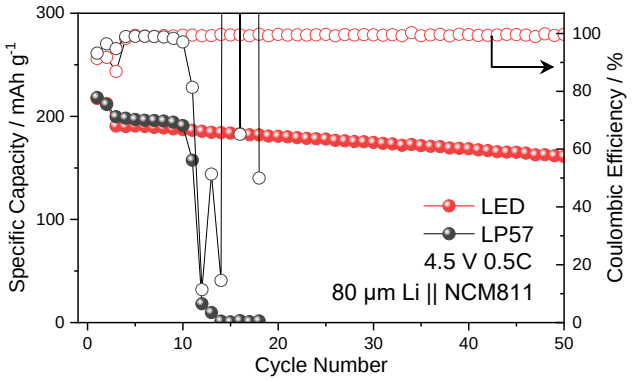

Fig. S9 Cycle performance of LED and LP57 electrolyte in the 80 μm Li || NCM811 full cell operated at 4.5 V and 0.5C. We find that the discharge capacity of the full cell using the traditional LP57 commercial electrolyte declined fast around the tenth cycle. The failure of this cell could be attributed to the incompatibility between the lithium metal anode and the carbonate solvent in the LP57 electrolyte operated at the high voltage. The excessive reduction and decomposition of the carbonate solvent could cause rapid decay of the cell performance.

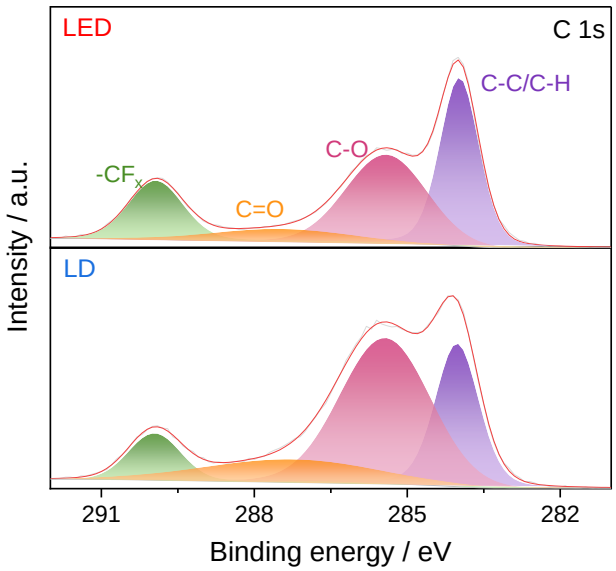

Fig. S10 XPS characterization of C 1s spectra for CEI components on cycled NCM811 cathode.

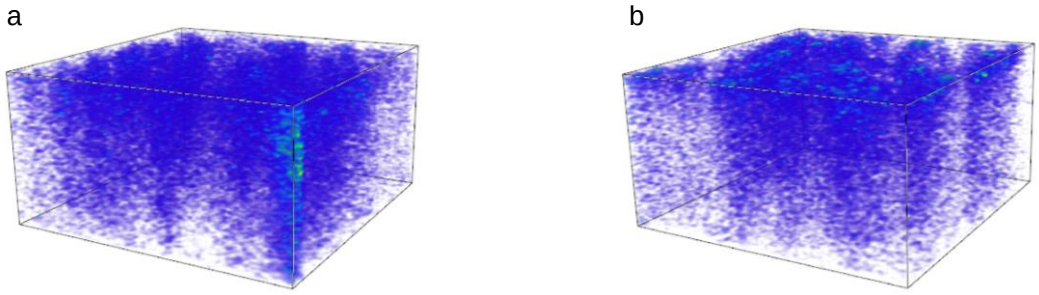

Fig. S11 The 3D rendering image of CHF_2^- using (a) LD and (b) LED electrolytes.

Supporting References:

1 Y. Zou, G. Liu, Y. Wang, Q. Li, Z. Ma, D. Yin, Y. Liang, Z. Cao, L. Cavallo, H. Kim, L. Wang, H. N. Alshareef, Y.-K. Sun and J. Ming, *Adv. Energy Mater.*, 2023, **13**, 2300443.

2 M. J. Frisch, G.W. Trucks, H.B. Schlegel, G.E. Scuseria, M.A. Robb, J.R. Cheeseman, G. Scalmani, V. Barone, G.A. Petersson, H. Nakatsuji, X. Li, M. Caricato, A.V. Marenich, J. Bloino, B.G. Janesko, R. Gomperts, B. Mennucci and D.J. Hratch. Gaussian 16, Revision C.01 *Gaussian, Inc., Wallingford CT,* 2016.

3 Y.-L. Wang, F. U. Shah, S. Glavatskih, O. N. Antzutkin and A. Laaksonen, *The Journal of Physical Chemistry B*, 2014, **118**, 8711-8723.

4 M. J. Abraham, T. Murtola, R. Schulz, S. Páll, J. C. Smith, B. Hess and E. Lindahl, *SoftwareX*, 2015, **1-2**, 19-25.

5 K. Tasaki and S. J. Harris, *J. Phys. Chem. C,* 2010, **114**, 8076-8083.